Chapter 2

FEMTOSECOND LASER DEVELOPMENT

Franz X. Kärtner[1], Erich P. Ippen[1] and Steven T. Cundiff[2]
[1]Research Laboratory of Electronics, Massachusetts Institue of Technology

[2]JILA, National Institute of Standards and Technology and University of Colorado

Abstract: Advances in ultrashort-pulse laser technology have led to few-cycle-duration optical pulses, with octave-spanning spectra, generated directly from laser oscillators at high repetition rates. These new laser systems promise to be reliable sources of carrier-envelope–phase-stabilized femtosecond pulse trains and highly stable laser frequency combs. In this chapter, we review the pulse and carrier-envelope phase dynamics of these laser sources and discuss different laser designs based on prismless cavities and cavities including prism pairs for dispersion compensation.

Key words: mode-locked lasers, carrier-envelope phase, frequency comb

1.   INTRODUCTION

Remarkable progress in the generation of femtosecond pulses with solid-state lasers has followed from the discovery of self-mode-locking in a Ti:sapphire laser by the Sibbett group in 1991 [1]. Explained as a consequence of self-focusing inside the laser [2], this self-mode-locking behavior has become known as Kerr-lens mode locking (KLM). It is now the basis for femtosecond pulse generation in a wide variety of other solid-state laser systems as well. As shown in Figure 2-1, KLM has resulted in the shortest pulses, superceding previous marks set using dye lasers, amplification, and spectral broadening.

Self-focusing in the KLM laser in the presence of aperturing due either to the size of the gain spot or some other physically introduced aperture can cause pulse shortening in precisely the manner described by "fast saturable absorber" mode-locking theory [3]. In addition, simultaneously occurring self-phase modulation (SPM), in the presence of group-velocity dispersion (GVD) in the resonator, provides a strong soliton like shaping to the pulses. This latter process can, in fact, be the dominant pulse-shaping effect;

however, the KLM remains necessary to suppress the growth of noise between the pulses, thereby stabilizing the mode locking. An important variant of soliton shaping occurs when the GVD alternates between positive and negative values as the pulse propagates. The result can be the formation of "dispersion-managed solitons" even when the average GVD in the resonator is zero or net normal [4]. Such dispersion management has found important application in "stretched-pulse" fiber lasers [5] and may also play a role in very short pulse Ti: sapphire lasers [6].
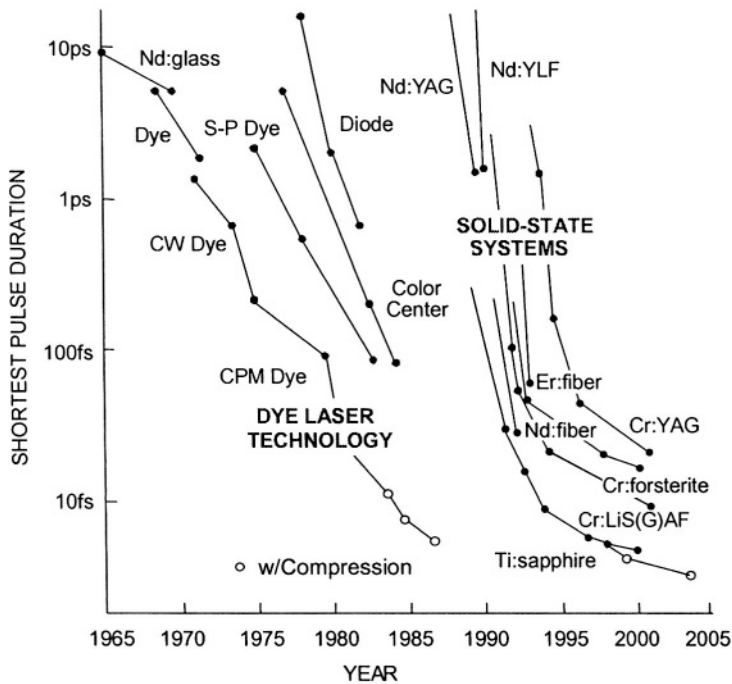

Figure 2-1. History of ultrashort pulse duration.

Ultrashort pulse durations have been reduced to well below 10 fs by a variety of researchers including the university groups at Washington State University [7], the Technical Universiy of Vienna [8], ETH-Zurich [9], the Massachusetts Institute of Technology (MIT) [10], and the University of Karlsruhe [11]. The Washington State group, responsible for a number of successful early cavity designs, first documented the limitations to pulse shortening by higher-order dispersion. The TU-Vienna group introduced chirped mirrors for dispersion compensation, an approach that was further refined at ETH-Zurich with the concept of a double-chirped mirror design. Dispersion compensation over one octave, ultimately achieved by the use of double-chirped mirror pairs at MIT and the University of Karlsruhe, finally

led to the generation of 5 fs pulses containing less than two optical cycles. The wings of the spectrum of these pulses extend over more than one octave, an achievement that has important implications for the control of the electric field waveform of the pulse. It had been recognized earlier by Xu et al.[12] that for few-cycle pulses, the maximum electric field in a pulse quantitatively depends on the phase relationship between the carrier wave and the maximum of the envelope (see Figure 2-1).

Nonlinear optical processes, which depend on powers of the electric field amplitude, must therefore also depend on the carrier-envelope phase for very short pulses. This dependence is visualized in Figure 2-2, which shows sketches of spectra resulting from instantaneous $\chi^{(2)}$ and $\chi^{(3)}$ processes produced by a chirp-free pulse with a rectangular-shaped spectrum spanning an octave. For a one-octave pulse, the spectra of the second-harmonic and optical-rectification terms overlap with the fundamental spectrum. Interference in the overlap regions will be constructive or destructive depending on the carrier-envelope phase. Use of this interference for carrier-envelope phase control is called the ν-to-2ν self-heterodyne technique. If higher-order processes are employed, such as a $\chi^{(3)}$ nonlinearity, there are similar interference terms between the $\chi^{(2)}$ and $\chi^{(3)}$ terms. Thus a phase-dependent interference is already possible even if the pulse spans only 2/3 of an octave. All of these interferences have been used to detect and control the carrier-envelope phase.
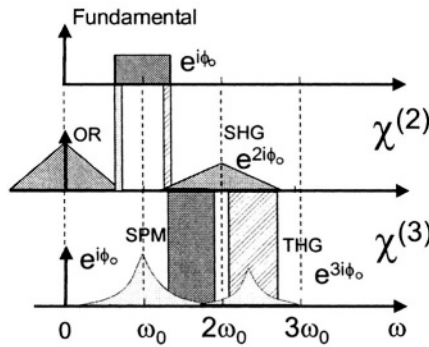

Figure 2-2. Top: Fundamental spectrum of an octave-spanning pulse centered at ω_0; Below: Spectra generated by instantaneous second- and third-order nonlinearities due to optical rectification (OR), second-harmonic generation (SHG), self-phase modulation (SPM), and third-harmonic generation (THG).

A special case, pointed out by Baltuška et al. [13], is that optical rectification or difference-frequency mixing of an optical pulse directly produces a phase-independent IR pulse. Currently, control of the carrier-

envelope phase for a variety of applications is one of the strongest motivations for the development of ultrabroadband lasers.

This chapter reviews progress made in phase-stabilized–octave-spanning lasers, starting with a discussion of the dispersion-managed pulse dynamics in sub-10 fs Ti:sapphire lasers in Section 2. In Section 3, the experimental realization of systems using combinations of prism pairs and chirped mirrors for dispersion compensation and prismless systems are described. Section 4 discusses the carrier-envelope phase dynamics of some sources. The results achieved are summarized in Section 5.

2. PULSE DYNAMICS

The generation of ultrashort pulses from Ti: sapphire lasers has progressed rapidly over the past decade and led to the generation of pulses as short as 5 fs directly from the laser. The spectra generated by these lasers are not of simple shape [7, 11, 14], and various models to explain this complexity have been presented. Christov et al. [15] have shown by numerical simulations that, when the second-order group-velocity dispersion is balanced, fourth-order dispersion with gain bandwidth filtering and KLM action can lead to steady-state pulse generation. Extensive three-dimensional simulations have been carried out [15-17]. However, so far, a fully three-dimensional numerical simulation of a KLM laser is still too time consuming for computation of the steady-state solution. Also, the solution is known from experimental observation to be very sensitive to changes in the self-focusing dynamics caused by slight parameter variations. This sensitivity adds to the difficulty of obtaining meaningful information from steady-state simulations that require many hours of computer time.

A schematic setup of current 5 fs Ti:sapphire lasers using only chirped mirrors for dispersion compensation is shown in Figure 2-3(a). For insight into the dynamics of this laser, we start by considering only the temporal dynamics, which are modeled by the nonlinear Schrödinger equation

$$\frac{\partial}{\partial z}a = -iD(z)\frac{\partial^2}{\partial t^2}a + i\delta(z)|a|^2 a \,, \tag{1}$$

describing propagation of the envelope function a in a medium with distributed dispersion, $D(z)$, and self-phase modulation, $\delta(z)$. The distribution of dispersion and nonlinearity in the laser is sketched in Figure 2-3(b). It was first pointed out by Spielmann et al. that for very-short-pulse Ti:sapphire lasers, large changes in the pulse occur within one round trip and

that the ordering of the pulse-shaping elements within the cavity has a major effect on the pulse formation [18]. The discrete action of linear dispersion in the arms of the laser resonator and the discrete, but simultaneous, action of positive SPM and positive GDD in the laser crystal cannot be neglected any longer. The importance of the strong variations in dispersion was first discovered in a fiber laser and called stretched-pulse mode locking [19]. The positive dispersion in the Er-doped fiber section of a fiber ring laser was balanced by a negative-dispersion passive fiber. The pulse circulating in the ring was stretched and compressed by as much as a factor of 20 in one round trip. One consequence of this behavior was a dramatic decrease of the nonlinearity and thus increased stability against the SPM-induced instabilities. Also, the formation of Kelly sidebands [20] occurring for large nonlinear phase shifts per round trip in conventional soliton lasers was greatly suppressed. The energy of the output pulses could be increased a hundredfold [21]. These important consequences can explain the high power densities that can be achieved in sub-10 fs KLM lasers without undergoing catastrophic self-focusing in the laser crystal.
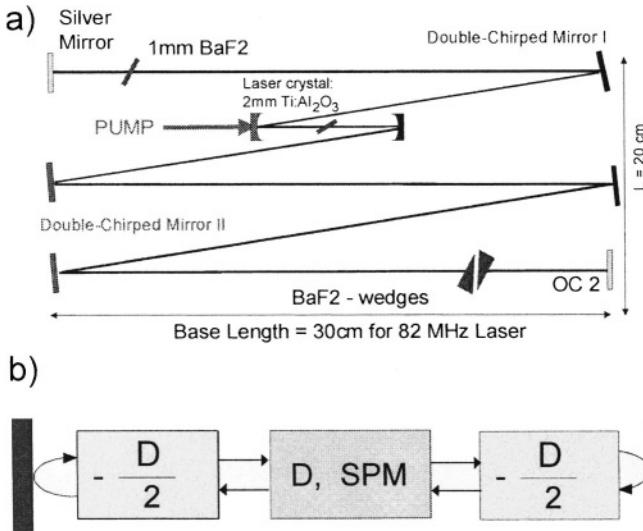

Figure 2-3. (a) Schematic of a Kerr-lens–mode-locked Ti:sapphire laser using double-chirped mirrors and BaF_2 for dispersion compensation. (b) Distribution of dispersion and nonlinearity inside the laser cavity.

Here, we consider the impact of the discrete action of dispersion and nonlinearity, which become important in the sub-10 fs range, in Ti:sapphire

lasers on the spectral shape of the laser pulses. The dispersion distribution shown in Figure 2-3(b) suggests an analogy with pulse propagation along a dispersion-managed fiber transmission link [4]. A system with sufficient variation of dispersion can support waves that have been called nonlinear Bloch waves [22]. One can show that the Kerr nonlinearity produces a self-consistent nonlinear scattering potential that permits formation of a periodic solution with a simple phase factor in a system with zero net dispersion. It has been shown further that nonlinear propagation along dispersion-managed fiber near zero net GDD possesses a narrower spectrum in the segment of positive dispersion than in the segment of negative dispersion [4, 22]. Thus, the effect of negative dispersion is greater than that of the positive dispersion, and the pulse sees an effective net negative dispersion. This effective negative dispersion can balance the Kerr-induced phase, leading to steady-state pulses at zero net dispersion. This is true even when there is no nonlinearity in the negative dispersion segment. The pulses are analogous to solitons in that they are self-consistent solutions of the Hamiltonian (lossless) problem as are conventional solitons. But, they are not secant hyperbolic in shape. Figure 2-4 shows a numerical simulation of a self-consistent solution of the Hamiltonian pulse-propagation problem in a linear medium of negative dispersion and subsequent propagation in a nonlinear medium of positive dispersion with positive self-phase modulation following Equation (1).

The dispersion map $D(z)$ is shown as an inset in Figure 2-5. The dispersion coefficient $D(z)$ and the nonlinear coefficient $\delta(z)$ are defined per unit length. In Figure 2-4, the steady-state intensity profiles are shown at the center of the negative dispersion segment over 1000 round trips. In addition, we can include in the model the saturable gain, Lorentzian gain filtering, and KLM modeled by a fast saturable absorber. Figure 2-5 shows the behavior in one period (one round trip through the resonator) including these effects. The response of the absorber is $q(a) = q_0 / \left(1 + |a|^2 / P_A\right)$, with $q_0 = 0.01$/mm and $P_A = 1$ MW. The bandwidth-limited gain is modeled by a Lorentzian gain profile with bandwidth $\Omega_g = 2\pi \times 43\,\text{THz}$. The filtering and saturable absorber reduce the spectral and temporal side lobes of the Hamiltonian problem, respectively, as can be inferred from Figures 2-4 and 2-5. The steady-state pulse formation can be understood in the following way: By symmetry, the pulses are chirp free in the middle of the dispersion cells. A chirp-free pulse starting in the center of the gain crystal, i.e., nonlinear segment, is spectrally broadened by the SPM and disperses in time because of the GVD, which generates a mostly linear chirp over the pulse.
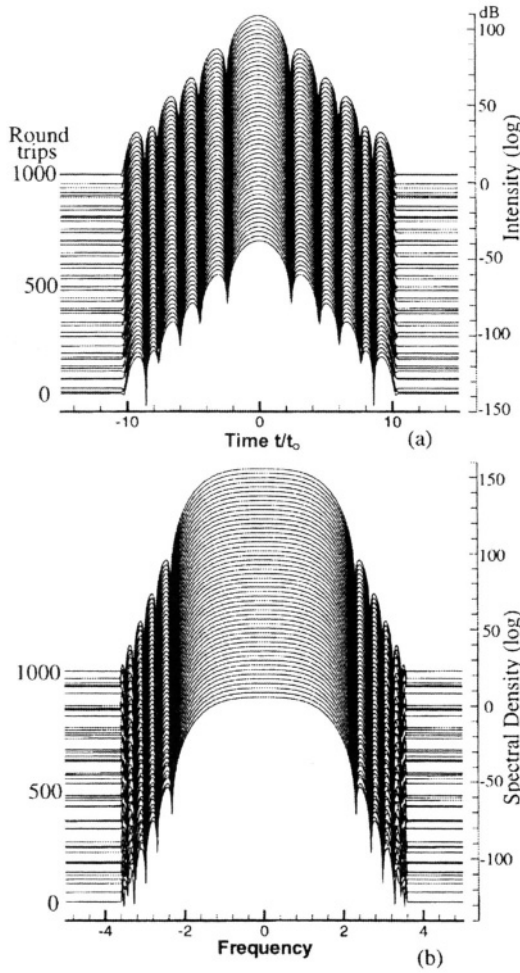
Figure 2-4. Simulation of the Hamiltonian problem. Temporal (a) and spectral (b) intensity profiles at the center of the negatively dispersive segment are shown for successive round trips. The total extent in 1000 round trips. $D = D^{(\pm)} = \pm 60$ fs/mm for the segment of crystal length $L = 2$ mm, $\tau_{FWHM} = 5.5$ fs, $\delta = 0$ for $D < 0$, $\delta = 1$ (MW-mm) for $D > 0$.
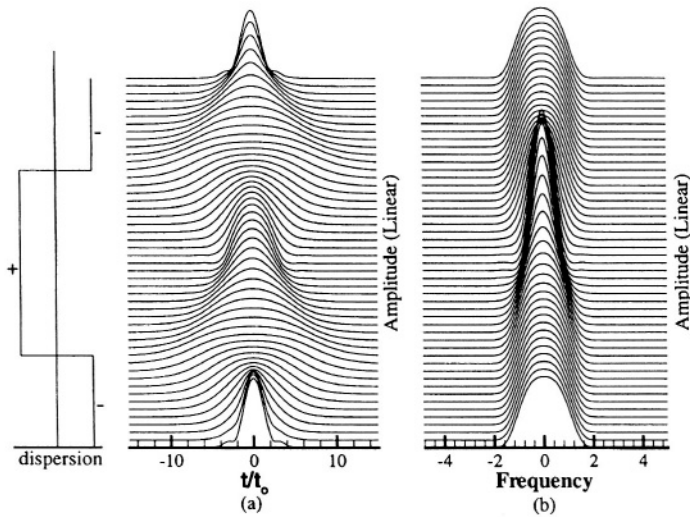
Figure 2-5. Pulse shaping in one round trip. The negative segment has no nonlinearity.

After the pulse leaves the crystal, it experiences GVD in the arms of the laser resonator. The positively chirped pulse is compressed to its transform limit at the end of each arm, where output couplers can be placed. Propagation back towards the crystal imposes a negative chirp, generating the time-reversed solution of the nonlinear Schrödinger Equation (1). Therefore, subsequent propagation in the nonlinear crystal compresses the pulse spectrally and temporally to its initial shape in the center of the crystal. The spectrum is narrower in the crystal than in the negative-dispersion sections, because it is negatively prechirped before it enters the SPM section. Spectral spreading occurs again only after the pulse has been compressed. This result further explains that in a laser with a linear cavity, for which the negative dispersion is located in only one arm of the laser resonator (i.e., in the prism pair and no use of chirped mirrors), the spectrum is widest in the arm that contains the negative dispersion [18]. In a laser with a linear cavity, for which the negative dispersion is equally distributed in both arms of the cavity, the pulse runs through the dispersion map twice per round trip. The pulse is short at each end of the cavity, and, most importantly, the pulses are identical in all passes through the crystal; thus they can exploit the full KLM action twice per round trip [23]. For this reason, a symmetric dispersion distribution may lead to an effective saturable absorption that is twice as strong as an asymmetric dispersion distribution and that can produce substantially shorter pulses. Furthermore, the dispersion swing between the negative and positive dispersion sections is only half as large, which allows

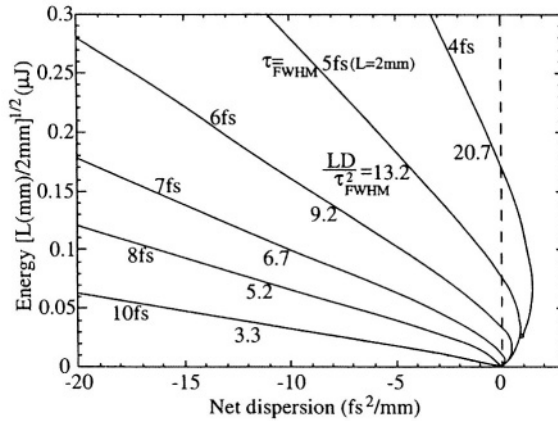for shorter dispersion-managed solitons operating at the same average power level.

Figure 2-6. Energy of the pulse in the lossless dispersion-managed system with stretching $S = LD/\tau^2_{FWHM}$ or, for a fixed crystal length L and pulse width as parameters; $D = 60$ fs^2/mm for Ti:sapphire at 800 mm.

A major difference from conventional soliton formation is illustrated in Figure 2-6. The figure shows the parameter ranges for a dispersion-managed Hamiltonian system (no gain, no loss, no filtering) that is unbalanced by the net dispersion that serves as the abscissa of the figure. Each curve gives the locus of energy vs net cavity dispersion for a stretching ratio $S = LD/\tau^2_{FWHM}$ (or pulse width with fixed crystal length L). One can see that for a pulse width longer than 8 fs with crystal length $L = 2$ mm, no solution of finite energy exists in the dispersion-managed system for zero or positive net dispersion. Pulses of durations longer than 8 fs require net negative dispersion. Hence, one can reach the ultrashort operation at zero net dispersion only by first providing the system with negative dispersion. At the same energy, one can form a shorter pulse by reducing the net dispersion, provided that the 8 fs threshold has been passed. For a fixed-dispersion swing ± *D,* the stretching increases quadratically with the spectral width or the inverse pulse width. Long pulses with no stretching have a sech shape. For stretching ratios of 3–10, the pulses are Gaussian shaped. For even larger stretching ratios, the pulse spectra become increasingly more flat topped, as shown in Figure 2-4.

These dynamics explain why there are steady-state pulses even at zero and slightly positive linear intracavity dispersion as confirmed in the experiment. These pulses would, of course, be unstable in the presence of

gain filtering due to the finite gain bandwidth of Ti:sapphire and, therefore, there is a need for strong-saturable-absorber action to keep the pulse stable against continuum radiation exploiting the peak of the gain. This saturable-absorber action is due to the Kerr-lens effect and can be optimized by various techniques [23, 24], which shall not be repeated here. Also, the spectral shape of the output pulses is greatly distorted because of the finite bandwidth of the output coupler, which can greatly enhance the wings of the laser spectrum, as we will see in the next section.

3. OCTAVE-SPANNING LASERS

Although an octave of spectrum can be generated by spectral broadening in microstructure fiber, there are advantages to using a laser that generates an octave directly. Since there is no medium with a gain spectrum that spans an octave (for Ti:sapphire, it approaches a half-octave), an octave-spanning laser clearly must rely on nonlinear broadening inside the laser cavity. The first demonstration of an octave-spanning laser used a second time-and-space focus in a separate glass element to enhance the nonlinearity [11]. More recently, there have been several demonstrations of Kerr-lens–mode-locked Ti:sapphire lasers that use the Ti:sapphire alone as the nonlinear medium. In this section, we discuss an implementation that uses intracavity prisms for dispersion compensation [25] and one that only uses dispersion-compensating mirrors [26].

The primary advantage of using an octave-spanning laser is that, by eliminating the microstructure fiber [27], issues of coupling and damage are also eliminated. Since the microstructure fiber has a very small core, the coupling is very alignment sensitive and tends to degrade with time. This poses a limit of approximately 10 hours on the duration of experiments. Although long enough for many applications, a proper clock needs to be able to run for days or longer. Damage to the microstructure fiber also limits the durations of experiments. However, there is significant variability as to how long it takes for damage to occur. Under some conditions, the fiber only lasts for hours, while under others it seems to last for weeks.

For time-domain experiments that are affected by carrier-envelope phase, it is important to maintain a short (transform-limited) pulse. The large higher-order dispersion in the fiber coupled with high nonlinearity essentially makes this impossible, whereas with an octave-spanning laser, it is possible.

With these advantages also come some disadvantages. The very high intracavity peak powers needed to obtain sufficient nonlinear spectral broadening makes these lasers susceptible to damaging the Ti:sapphire

crystal. This damage takes some time to occur but can limit the duration of experiments. In addition, the output spatial mode exhibits strong frequency dependence, which can also impact experiments.

Intracavity continuum generation has been demonstrated in a Ti:sapphire laser that was operated in the self-Q-switching regime [28]. However, in this regime, the spectrum is unstable and therefore not useful for femtosecond comb applications. As described in Chapter 3, intracavity continuum generation has also been observed in high-repetition-rate lasers [29], but there was insufficient power at the octave points to implement ν-to-2ν stabilization. A 2ν-to-3ν scheme had to be used [30].

Finally, we would like to comment on the definition of "octave spanning." The span of a spectrum is often taken as the width at some power below the peak (often full-width at half-maximum or perhaps even at the 10 dB points). However, for femtosecond comb applications, there is a good operational definition of octave spanning, namely that it is possible to obtain ν-to-2ν beats. A slightly stronger version of this is that the beats are sufficiently strong to be used to stabilize the offset frequency of the laser. This criterion can be met even when the intensity at the octave points is as much as 40 dB below the peak.

3.1   Octave-spanning laser using prisms

The early designs for broadband Kerr-lens–mode-locked Ti:sapphire lasers [31] used a two-prism sequence for dispersion compensation [32]. Some mechanism for generating anomalous dispersion is needed to correct for the chirp acquired by the pulse as it passes through the normal dispersion Ti:sapphire crystal (and air for extreme bandwidth). The development of dispersion-compensating mirrors (also called "chirped mirrors") [33], which have anomalous dispersion, meant that broadband mode locking could be achieved without prisms [34]. Dispersion-compensating mirrors not only provide anomalous dispersion, but they also have a much larger reflection bandwidth than standard dielectric mirrors. Incorporating both prisms and dispersion-compensating mirrors added additional flexibility in the design and enabled the production of sub-two-cycle pulses [10]. In this section, an octave-spanning laser that incorporates both prisms and dispersion-compensating mirrors is presented. To meet the operational definition of "octave spanning," we show that clean ν-to-2ν beats can be obtained and used to lock the offset frequency of the laser comb.

3.1.1 Design

The prism-based–octave-spanning Ti:sapphire laser is an x-folded cavity that uses commercially available negatively chirped mirrors and intracavity CaF_2 prisms for dispersion compensation, as shown in Figure 2-7. M1 and M2 (10 cm radius of curvature) are both double-chirped mirrors (DCM) designed to be used with CaF_2 prisms [10]. M3 and EM are both negatively chirped Layertec™ mirrors,[*] part numbers 100466 and 101515, respectively. The output coupler (OC) is G034-007 from Spectra Physics[*] and the prism separation between the two CaF_2 prisms is ~82 cm. The laser crystal is 2.3 mm long and the pump focusing lens has a focal length of 10 cm. When the laser is pumped with 5.5 W of 532 nm light, the spectrum, at its broadest, extends from ~570 to ~1280 nm (-35 dB from the 800 nm portion of the spectrum). The average ML power is > 400 mW (100 mW cw) at an 88 MHz repetition rate. Mode locking is easily initiated by quickly changing the insertion of the prism furthest from EM.
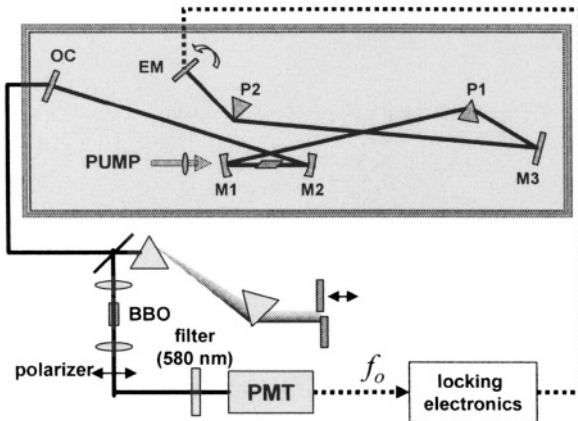

Figure 2-7. Schematic of laser and v-to-2v detection of f_0.

The continuum generated by the laser relies on the interplay between an enhancement of SPM and dispersion compensation, where the latter allows for the existence of the former. The exact choice of chirped mirrors, the prism separation, and the prism insertion appear not to be very important. Different combinations of mirrors for M1 and M2 (Layertec 101568), M3 (DCM, Layertec 100466 and 101515) and EM (Layertec 100466 and

---

[*] This information is given for technical purposes only and does not represent an endorsement on the part of the National Institute of Standards and Technology.

101515), and a protected silver mirror were tested and yielded octave-spanning spectra. Also, two OC's (Spectra Physics G034-007 and CVI Laser PR2 — 2% transmission @ 800nm) resulted in an octave of bandwidth. We have not been able to reproduce the octave spectrum using fused silica prisms. Apparently, in this case, the continuum generation does not result from meticulous dispersion compensation. This is not surprising since the continuum is created on a single pass through the crystal. As a result, careful dispersion compensation may only be necessary over the bandwidth indicated by the OC reflectivity and not the entire spectrum.

The position of the curved mirrors is critical for producing an octave-spanning spectrum. Typically, KLM is obtained by displacing one curved mirror away from the optimum mirror position for cw operation. Here, the mirror furthest from the pump is translated inward to the point that the laser is on the edge of stability for cw operation. This arrangement increases the discrimination between mode-locked and cw operation and requires the formation of a strong Kerr-lens to correct for the misalignment with respect to the pump. To optimize the bandwidth, both curved mirrors are then translated in the same direction away from the pump, just before the point where the laser begins Q-switching.

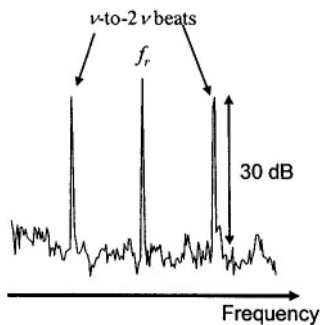### 3.1.2 Carrier-envelope phase stabilization

Figure 2-8. Rf spectrum showing a repetition rate peak and v-to-$2v$ heterodyne beats.

To measure and stabilize the carrier-envelope phase in this laser, we implement the simplest self-referencing scheme, which compares the second harmonic on the low frequency extreme of the laser spectrum with the fundamental on the extreme high end of the spectrum (see Chapter 2). A v-to-$2v$ interferometer is used to measure f_0. Specifically, f_0 is obtained via optical heterodyne between the fundamental light of the laser spectrum at ~580 nm and doubled light at ~1160 nm, see Figure 2-7. For the

measurements presented here, the signal-to-noise ratio of the offset-frequency beat note, using the octave spectrum (see Figure 2-8), is greater than 30 dB at 100 kHz resolution bandwidth. Once measured, f_0 is then stabilized by actively tilting the end mirror (EM) [35] with an in-loop-accumulated phase error of 0.18 rad (1.65 mHz–102kHz), as shown in Figure 2-8. Because this is an in-loop measurement of the phase noise, it therefore may not be used alone to characterize the noise on the output of the laser. However, using the octave spectrum from the laser directly, we have eliminated the out-of-loop phase noise generated by microstructure fiber [36]. Also, because the prism-based ν-to-2ν interferometer used in the measurement of f_0 minimizes non-common-mode mirrors, the dominant source of out-of-loop phase noise on the laser results from the feedback electronics.
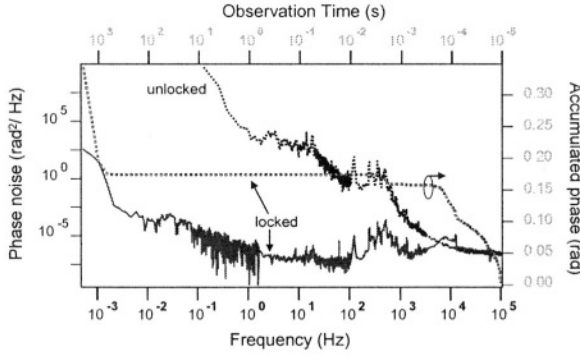

Figure 2-9. Power spectral density of phase noise (left axis) and accumulated rms phase fluctuations (right axis).

3.1.3 Frequency-dependent spatial mode

Since the light in the wings of the spectrum is generated by self-phase modulation and is outside the gain bandwidth, it is not truly lasing and does not have to obey resonance conditions in the cavity. This means the spatial mode in the wings can vary significantly. This variation is relevant to f_0 detection as it can degrade the spatial-mode matching and thus limit the signal-to-noise ratio of the f_0 beat note. It may also pose problems to pulse compression. This mismatch in mode profiles is depicted Figure 2-10. Figure 2-11 shows the result of a 90/10 knife-edge method that was used to perform a second moment measurement of the beam profiles to yield the beam spot sizes as a function of wavelength [37]. From this result, we see that the spectral extremes exhibit a significant increase in asymmetry and deviation

away from the resonant Gaussian TEM_{00} mode and its corresponding $1/\lambda$ diffraction limit.
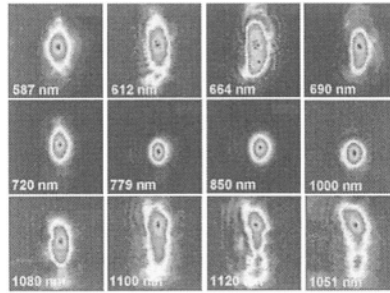

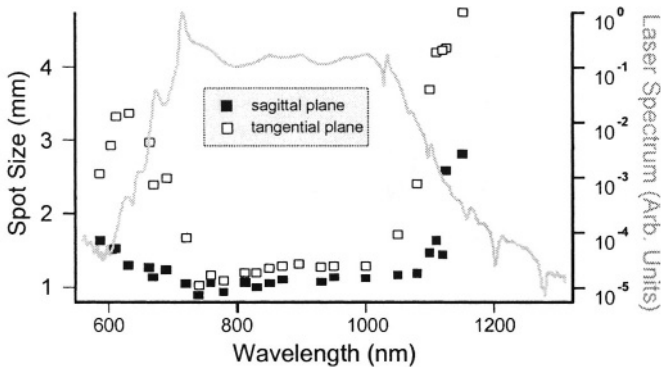*Figure 2-10.* Beam profiles at various wavelengths.

Figure 2-11. Measured sagittal and tangential spot sizes as a function of wavelength (squares, left axis). Line shows laser spectrum (right axis).

Measurement of the beam parameters at the output coupler, as shown in Figure 2-12, explains the increase in spot size in the wings of the spectrum. The beam waist shows a sudden decrease of the nonresonant as compared to the resonant modes. This decrease should cause a greater divergence in the wings of the laser spectrum, thereby leading to the larger spots sizes observed in the far field (see Figure 2-10). Figure 2-13 compares the measured beam divergence to that which would result from the propagation of a Gaussian TEM_{00} mode given the respective measured beam waists in Figure 2-12. The ratio of the former to the latter gives the M^2 value as a function of wavelength, indicating the strength of the non-TEM_{00}-Gaussian beam propagation (non-Gaussian modes and/or higher modes).
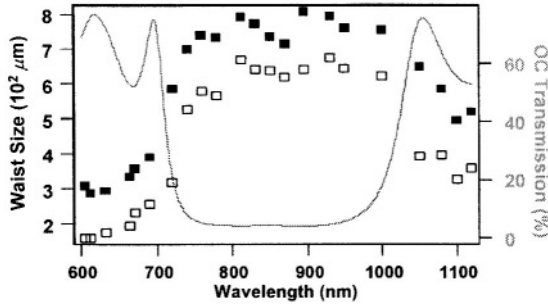
Figure 2-12. Waist size at output coupler as a function of wavelength for sagittal and tangential planes (squares, left axis). Output coupler transmission is line (right axis).
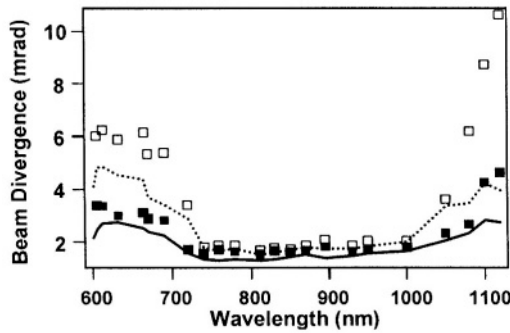

Figure 2-13. Measurement of beam divergence (squares) and predicted divergence based on waist size (lines).

The mode profiles and the sudden decrease in waist in the extremes of the spectrum still need to be explained. For resonant modes, the cavity geometry determines the waist size and divergence. The beam characteristics of the nonresonant modes, however, can be directly influenced by the Kerr lens in the crystal and by diffraction and aperturing of optics without the self-correcting effects of the cavity. The Kerr lensing is considerable since intracavity continuum generation, for this laser, requires significant realignment away from ideal cw operation. This realignment results in a highly asymmetric cw beam (tangential waist/sagittal waist = 1.56) and a large discrimination in average output power between cw and mode-locked operation (4:1). The asymmetry implies that the nonlinear correction for the cw asymmetry may result in the formation of an asymmetric Kerr lens, which may explain the observed asymmetry in the wings of the spectrum. This mirror positioning also results in a different initial cw condition than for

"normal" KLM because it gives rise to a much more tightly focused cw beam than the pump beam (~ ratio of 4:1, calculated using ABCD cavity propagation based on the observed cw asymmetry). This leads us to the conclusion that the effect of the Kerr lens should be one that increases the waist of the mode-locked beam. The increased waist size improves the efficiency with which power is extracted from the pump beam and thus still acts as an effective saturable absorber. This is consistent with the observed beam waists (Figure 2-12), as the frequency at the very edges of the spectrum should be produced by a weaker Kerr lens than those of the resonant modes [37]. Complete modeling of the relationship between nonlinear effects in the crystal and pulse formation, however, is beyond the scope of this chapter but has been addressed elsewhere [16].

3.2   Prismless octave-spanning laser

We have also built octave-spanning lasers where dispersion compensation is completely achieved by double-chirped mirror pairs [38] and thin BaF_2 wedges for fine adjustment of the dispersion [26, 39]. Prismless lasers do have the advantage of being scalable to GHz repetition rates because of the compact dispersion compensation via chirped mirrors. Higher repetition rates mean higher power per mode at the same average output power, which is advantageous for frequency metrology. Also, the compactness of the cavity makes it less sensitive to temperature variations and environmental perturbations.

3.2.1 Design

The lasers consist of astigmatically compensated x- or z- folded cavities. The x-folded version is shown in Figure 2-14(a). The lasers have a 2 mm long Ti:sapphire crystal with an absorption of $\alpha = 7$ cm^{-1} at 532 nm. They are pumped by a diode-pumped, frequency-doubled Nd:vanadate laser. The radius of curvature (ROC) of the folding mirrors is 10 cm, and the pump lens has a 60 mm focal length. All mirrors in the cavity, with the exception of the end mirrors, are type I (gray) and type II (black) double-chirped mirrors (DCM) that generate smooth group-delay dispersion when used together in pairs [38]. Figure 2-9(b) shows the reflectivity and group delay of the DCM pairs. The total group delay is smooth from 600 to 1200 nm. The average reflectivity over the full octave can be as high as 99.9%. One cavity end mirror is a silver mirror and the other is a broadband output coupler, made of either $ZnSe/MgF_2$ (80 MHz repetition-rate laser) or TiO_2/SiO_2 (150 MHz repetition-rate laser) coatings with 1% transmission. The output power in cw operation is typically 40 mW with 4.4 W pump power. In mode-locked

operation, the average power is 90 mW. The output power is limited by low output coupling and scattering losses in the OC coating and the silver mirror. Presumably, further optimization of output coupling and elimination of the silver mirror would increase laser efficiency.
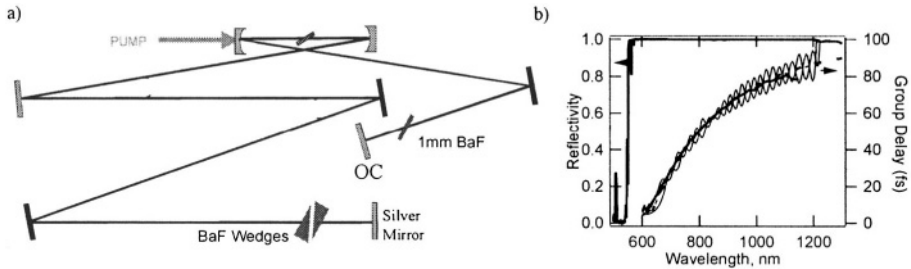

Figure 2-14. (a) Schematic diagram of octave-spanning prismless laser. Gray and black mirrors are type I and II double-chirped mirrors (DCMs), respectively. The BaF_2 wedges are used for fine-tuning of the dispersion, (b) Reflectivity (left scale) of the type I DCMs with pump window shown as thick solid line. The group-delay design is given by the thick, dash-dotted line. The individual group delays (right scale) of type I and II DCMs are shown as thin lines and the average as a dashed line (almost identical to the design goal over the wavelength range of interest from 650–1200 nm). The measured group delay, using white-light interferometry, is shown as the thick solid line from 600–1100 nm. Beyond 1100 nm, the sensitivity of the Si detector limited the measurement.

In one round trip of the laser pulse through the cavity, the total number of bounces on DCMs (12 bounces) generates the precise negative dispersion required to compensate for positive second- and higher-order dispersion caused by the laser crystal, the air path in the cavity, and the BaF_2 wedge pairs used to fine-tune the intracavity dispersion.

We used BaF_2 for dispersion compensation because it has the lowest ratio of third- to second-order dispersion in the wavelength range from 600–1200 nm, and the slope of the dispersion of BaF_2 is nearly identical to that of air. These features make it possible to scale the cavity length and repetition rate without changing the overall intracavity dispersion. To achieve mode-locked operation, it is necessary to reduce the amount of BaF_2 inside the laser cavity (by withdrawing one of the wedges).

The broadest spectrum can be achieved by optimizing the insertion of the BaF_2 wedge, so that the laser operates very close to the zero average-dispersion point. In this case, the spectral width of the laser is critically dependent on the dispersion balance. With the prismless lasers, adjusting the dispersion does not significantly change the cavity alignment. Figures 2-15(a) and (b) show the spectrum under broadband operation of an 80 MHz and a 150 MHz laser, respectively. The octave is already reached at a

spectral density about 25 dB below the average power level. The same plots
also show the corresponding OC transmission curves. The detailed shape of
this transmission curve is a determining factor in the width of the output
spectrum, since it significantly enhances the spectral wings. A roll-off of the
output coupler matched to the intracavity spectrum is necessary to generate
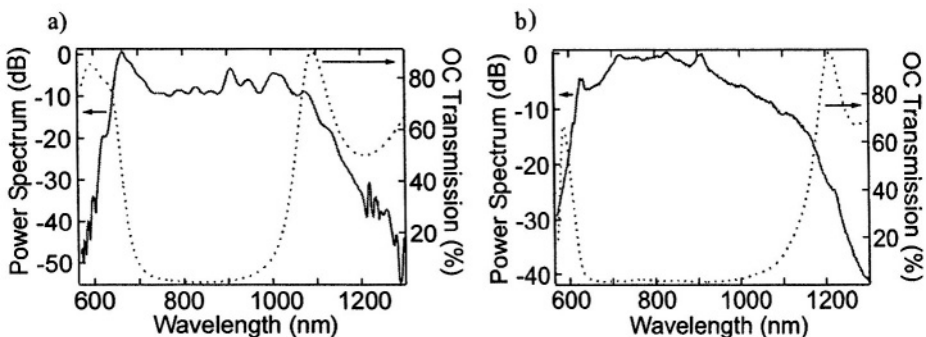the octave-spanning spectrum.

Figure 2-15. (a) Measured output spectra for lasers with 80 MHz repetition rate and (b) 150
MHz repetition rate. In both cases, the octave is reached at approximately 25 dB below the
average power level. The average mode-locked power is 90 mW for both lasers. Also shown
(dashed lines) are the respective output coupler (OC) transmission curves for the $ZnSe/MgF_2$
Bragg-stack (a) and a broadband SiO_2/TiO_2 stack (b). Both have about 1% transmission at
800 nm.

3.2.2   Carrier-envelope phase stabilization

We directly measure f_0 by the ν-to-2ν technique described earlier, as
shown in Figure 2-16(a). Using a dichroic beamsplitter, we split the laser
output into long- and short-wavelength components and recombine them
after insertion of a proper time-delay stage. The delay stage is essential to
compensate for the difference in group delay between the 580 and 1160 nm
radiation in the optical components (splitters, OC and BBO crystal). The
recombined beam is then focused into a 1 mm BBO crystal cut for type I
second harmonic of 1160 nm. The resulting output is sent through a 10 nm
wide spectral filter centered at 580 nm. After projecting the doubled 1160
nm light and the fundamental into the same polarization to enable
interference, the beat signal is detected by a photomultiplier tube (PMT).
Figure 2-16(b) shows the detected f_0 beat signals with 10 kHz and 100 kHz
measurement bandwidths. The signal-to-noise ratios are 30 dB and 40 dB,
respectively. The f_0 beat is very stable and the laser stays mode locked over
many days. In the absence of active feedback and without any temperature
control, the f_0 frequency stays within the bandwidth of the bandpass filter

following the PMT, which is 8MHz, for more than 10 hours. On the time scale of seconds, the beat can jitter by about 100 kHz. The f_0 lock only breaks because of a slow drift of the beat note out of the filter bandwidth of the 8 MHz filter, which is not yet controlled.
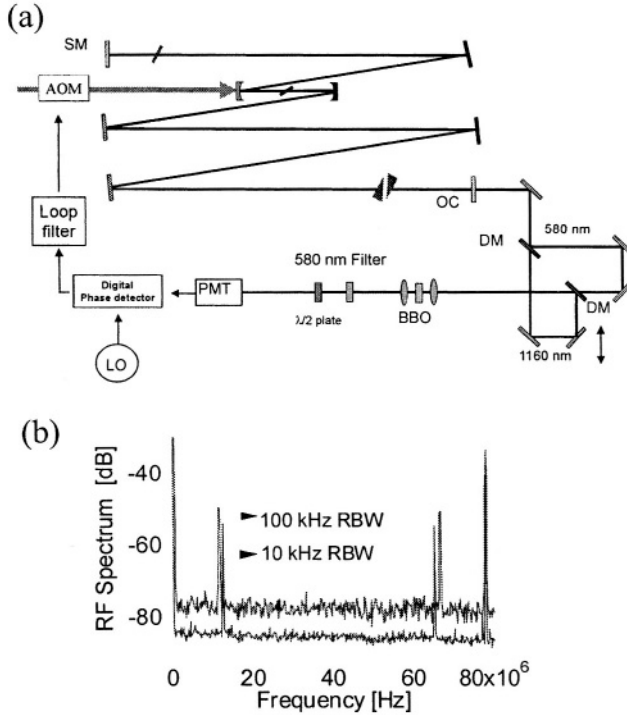

Figure 2-16. (a) Setup for f_0 detection and lock. (b) Measured carrier-envelope beat signal from the 80 MHz laser.

To demonstrate control over the comb, we filter the component $f_r + f_0$ at 130 MHz from the PMT signal and phase lock it to a stable rf synthesizer using a phase-locked loop. To increase the locking range, the 130 MHz component of the signal is properly filtered and amplified, sent to a thirty-two-fold frequency divider, and then compared with the synthesizer signal in a digital phase detector. The properly filtered and amplified phase-error signal controls the pump power via an acousto-optic modulator that directly controls the carrier-envelope frequency of the mode-locked laser.

Figure 2-17 shows the measured phase-error spectral densities of the f_0 beat with and without active stabilization. The integrated phase error for the in-loop measurement is 0.2 rad (from 1 Hz to 10 MHz). The major contribution to this phase-noise error comes from the yet unsuppressed pump noise. We expect further improvement in the residual carrier-envelope phase

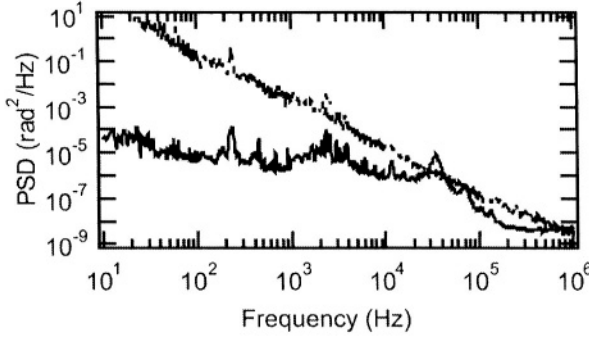fluctuations with an improved loop filter design for stronger noise suppression.

Figure 2-17. Spectral densities of the phase-error signal at the output of the digital phase detector for the f_0 lock (solid line) and free running f_0 (dashed line).

4. CARRIER-ENVELOPE PHASE DYNAMICS

The carrier-envelope phase evolution in a mode-locked laser depends on the pulse energy. This is not surprising as there is a nonlinear contribution to the phase shift of the intracavity pulse as it passes through the gain crystal. At the simplest level, this nonlinear phase shift happens because of the Kerr effect, i.e., the index of refraction depends on intensity and hence so does the optical path length. This is clearly an over simplification. Better insight is based on treating the pulse as a soliton. However, care is needed as classical soliton theory does not include the fact that the group velocity also depends on intensity (known as the "shock" term) or the fact that dispersion and nonlinearity in the laser are not constant as a function of position in the cavity. The intensity dependence of the carrier-envelope phase has both positive and negative aspects. On the positive side, it provides a parameter by which the carrier-envelope phase can be controlled. On the negative side, it means the amplitude noise will be converted to phase noise.

One of the first experiments to measure carrier-envelope phase evolution (using a cross-correlator) observed its intensity dependence [12]. However, the slope, $d\Delta\phi_{ce}/dI$, had the opposite sign from what was expected based on classical soliton theory. This result was explained as being caused by an intensity-dependent shift in the spectrum.

Subsequent theoretical work included the effect of the shock term [40]. It was found that the shock term causes the group velocity to change twice as fast with intensity as does the phase velocity. This fact results in an opposite sign of $d\Delta\phi_{ce}/dI$ from what it would be if the shock term were ignored.

Further experiments using self-referencing to detect $\Delta\phi_{ce}$ showed that $d\Delta\phi_{ce}/dI$ could actually change signs [41]. The results were consistent with the shifting of the spectrum with intensity also changing signs. These measurements also showed that for shorter pulses, $\Delta\phi_{ce}$ was much less sensitive to changes in the pulse intensity. This finding is consistent with theoretical work [40] but may also be simply due to clamping of the spectrum because of implicit spectral filtering in the laser.

Numerical simulations of nonlinear pulse propagation in sapphire also show a change in the sign of $d\Delta\phi_{ce}/dI$ that arises from warping of the envelope at high intensities [42]. There was no corresponding change in the direction of spectral shift, as was observed experimentally. However, this work only modeled propagation in sapphire and did not treat the rest of the laser cavity.

More recent theoretical treatment based on a multiple-scales treatment of dispersion-managed solitons included both managed dispersion and nonlinearity [43]. Both shock and third-order dispersion were considered as well. The results confirmed the earlier conclusions [40], although the details varied because of differences in the treatment of and inclusion of additional effects.

At this point, a number of phenomena have been identified in theory and experiment, although a clear connection between them remains elusive. A further understanding is important as these effects, which are used to control $\Delta\phi_{ce}$, can also corrupt its stability and hence that of the generated spectral comb.

5.   SUMMARY

The recent explosion in work on carrier-envelope phase stabilization of ultrashort pulses and the resulting stable frequency comb has been built on a foundation of mode-locked laser technology. The culmination of this has been the development of lasers that directly generate an octave-spanning spectrum. At the same time, the need for stabilization has pushed mode-locked laser technology in new directions and forced the development of an improved understanding of the lasers.

ACKNOWLEDGEMENTS

REFERENCES

[1]   D. E. Spence, P. N. Kean, and W. Sibbett, Opt. Lett. **16**, 42-44 (1991).
[2]   D. K. Negus, L. Spinelli, N. Goldblatt, and G. Feugnet, in *Advanced Solid-State Lasers* (OSA, 1991), Vol. 10; F. Salin, J. Squier, and M. Pichè, Opt. Lett. **16**, 1674-1676 (1991); M. Pichè, Opt. Commun. **86**, 156-160 (1991).
[3]   H. A. Haus, IEEE J. Quantum Electron. **11**, 736-746 (1975).
[4]   J. H. B. Nijhof, N. J. Doran, W. Forysiak, and F. M. Knox, Electron. Lett. **33**, 1726-1727 (1997).
[5]   K. Tamura, H. A. Haus, and E. P. Ippen, Electron. Lett. **28**, 2226-2228 (1992).
[6]   Y. Chen, F. X. Kärtner, U. Morgner, S. H. Cho, H. A. Haus, E. P. Ippen, and J. G. Fujimoto, J. Opt. Soc. Am. B **16**, 1999-2004 (1999).
[7]   J. P. Zhou, G. Taft, C. P. Huang, M. M. Murnane, H. C. Kapteyn, and I. P. Christov, Opt. Lett. **19**, 1149-1151 (1994).
[8]   A. Stingl, C. Spielmann, F. Krausz, and R. Szipocs, Opt. Lett. **19**, 204-206 (1994).
[9]   D. H. Sutter, G. Steinmeyer, L. Gallmann, N. Matuschek, F. Morier-Genoud, U. Keller, V. Scheuer, G. Angelow, and T. Tschudi, Opt. Lett. **24**, 631-633(1999).
[10]   U. Morgner, F. X. Kärtner, S. H. Cho, Y. Chen, H. A. Haus, J. G. Fujimoto, E. P. Ippen, V. Scheuer, G. Angelow, and T. Tschudi, Opt. Lett. **24**, 411-413 (1999).
[11]   R. Ell, U. Morgner, F. X. Kärtner, J. G. Fujimoto, E. P. Ippen, V. Scheuer, G. Angelow, T. Tschudi, M. J. Lederer, A. Boiko, and B. Luther-Davies, Opt. Lett. **26**, 373-375 (2001).
[12]   L. Xu, C. Spielmann, A. Poppe, T. Brabec, F. Krausz, and T. W. Hänsch, Opt. Lett. **21**, 2008-2010 (1996).
[13]   A. Baltuška, T. Fuji, and T. Kobayashi, Phys. Rev. Lett. **88**, art. no.-133901 (2002).
[14]   L. Xu, C. Spielmann, F. Krausz, and R. Szipocs, Opt. Lett. **21**, 1259-1261 (1996).
[15]   I. P. Christov, H. C. Kapteyn, M. M. Murnane, C. P. Huang, and J. P. Zhou, Opt. Lett. **20**, 309-311 (1995).
[16]   I. P. Christov, V. D. Stoev, M. M. Murnane, and H. C. Kapteyn, Opt. Lett. **21**, 1493-1495 (1996).
[17]   I. P. Christov and V. D. Stoev, J. Opt. Soc. Am. B **15**, 1960-1966 (1998).
[18]   C. Spielmann, P. F. Curley, T. Brabec, and F. Krausz, IEEE J. Quantum Electron. **30**, 1100-1114 (1994).
[19]   K. Tamura, E. P. Ippen, H. A. Haus, and L. E. Nelson, Opt. Lett. **18**, 1080-1082 (1993).

[20]   S. M. J. Kelly, Electron. Lett. **28**, 806-807 (1992); J. P. Gordon, J. Opt. Soc. Am. B **9**, 91-97 (1992).
[21]   K. Tamura, E. P. Ippen, and H. A. Haus, App. Phys. Lett. **67**, 158-160 (1995).
[22]   Y. Chen and H. A. Haus, J. Opt. Soc. Am. B **16**, 24-30 (1999).
[23]   R. Reinisch and G. Vitrant, Prog. Quantum Electron. **18**, 1-38 (1994).
[24]   E. J. Grace, A. Ritsataki, P. M. W. French, and G. H. C. New, Opt. Commun. **183**, 249-264 (2000).
[25]   T. M. Fortier, D. J. Jones, and S. T. Cundiff, Opt. Lett. **28**, 2198-2200 (2003).
[26]   L. Matos, O. Kuzucu, T. R. Schibli, J. Kim, E. P. Ippen, D. Kleppner, and F. X. Kärtner, Opt. Lett. **29** (2004).
[27]   J. K. Ranka, R. S. Windeler, and A. J. Stentz, Opt. Lett. **25**, 25-27 (2000).
[28]   J. P. Likforman, A. Alexandrou, and M. Joffre, App. Phys. Lett. **73**, 2257-2259(1998).
[29]   A. Bartels and H. Kurz, Opt. Lett. **27**, 1839-1841 (2002).
[30]   T. M. Ramond, S. A. Diddams, L. Hollberg, and A. Bartels, Opt. Lett. **27**, 1842-1844(2002).
[31]   M. T. Asaki, C. P. Huang, D. Garvey, J. P. Zhou, H. C. Kapteyn, and M. M. Murnane, Opt. Lett. **18**, 977-979 (1993).
[32]   R. L. Fork, O. E. Martinez, and J. P. Gordon, Opt. Lett. **9**, 150-152 (1984).
[33]   R. Szipocs, K. Ferencz, C. Spielmann, and F. Krausz, Opt. Lett. **19**, 201-203 (1994).
[34]   A. Stingl, M. Lenzner, C. Spielmann, F. Krausz, and R. Szipocs, Opt. Lett. **20**, 602-604(1995).
[35]   S. T. Cundiff, J. Ye, and J. L. Hall, Rev. Sci. Instrum. **72**, 3746-3771 (2001).
[36]   T. M. Fortier, J. Ye, S. T. Cundiff, and R. S. Windeler, Opt. Lett. **27**, 445-447 (2002).
[37]   S. T. Cundiff, W. H. Knox, E. P. Ippen, and H. A. Haus, Opt. Lett. **21**, 662-664(1996).
[38]   F. X. Kärtner, U. Morgner, R. Ell, T. Schibli, J. G. Fujimoto, E. P. Ippen, V. Scheuer, G. Angelow, and T. Tschudi, J. Opt. Soc. Am. B **18**, 882-885 (2001).
[39]   T. R. Schibli, O. Kuzucu, J. W. Kim, E. P. Ippen, J. G. Fujimoto, F. X. Kaertner, V. Scheuer, and G. Angelow, IEEE J. Sel. Top. Quantum Electron. **9**, 990-1001 (2003).
[40]   H. A. Haus and E. P. Ippen, Opt. Lett. **26**, 1654-1656 (2001).
[41]   K. W. Holman, R. J. Jones, A. Marian, S. T. Cundiff, and J. Ye, Opt. Lett. **28**, 851-853 (2003); K. W. Holman, R. J. Jones, A. Marian, S. T. Cundiff, and J. Ye, IEEE J. Sel. Top. Quantum Electron. 9, 1018-1024 (2003).
[42]   P. M. Goorjian and S. T. Cundiff, Opt. Lett. **29**, 1363 (2004).
[43]   M. J. Ablowitz, B. Ilan, and S. T. Cundiff, Opt. Lett. **29**, 1808-1810 (2004).